



Article

Self-Healing and Mechanical Behaviour of Fibre-Reinforced Ultra-High-Performance Concrete Incorporating Superabsorbent Polymer Under Repeated and Sustained Loadings

Mohammad Alameri ¹, M.S. Mohamed Ali ^{1,*}, Mohamed Elchalakani ², Abdul Sheikh ¹ and Rong Fan ³

¹ School of Architecture and Civil Engineering, The University of Adelaide, Adelaide, SA 5005, Australia; mohammad.alameri@adelaide.edu.au (M.A.); abdul.sheikh@adelaide.edu.au (A.S.)

² Department of Civil, Environmental and Mining Engineering, The University of Western Australia, Perth, WA 6009, Australia; mohamed.elchalakani@uwa.edu.au

³ Commonwealth Scientific and Industrial Research Organisation (CSIRO) Mineral Resources, Adelaide, SA 5064, Australia; rong.fan@csiro.au

* Correspondence: mohamed.mohamedsadakkathulla@adelaide.edu.au

Abstract: This study investigated the mechanical responses and self-healing capability of incorporating superabsorbent polymer (SAP) particles in Fibre-Reinforced Ultra-High-Performance Concrete (UHPC) mixes under repetitive flexural and sustained tensile loadings. UHPC with SAP addition of 0.3% and 0.4% of the binder ratio were studied along with a control UHPC mix. The methodology included investigating the mechanical properties of these mixes under ambient, water, and 100% of relative humidity (RH) curing conditions. In addition, the mechanical performance of ambient-, water-, and 100% RH-cured prismatic specimens (100 mm × 100 mm × 500 mm) under repeated load was studied under the same curing conditions. Prismatic specimens (75 mm × 75 mm × 500 mm) were kept under cure conditions of wet and dry cycles with applied tensile load for 28 days for the sustained tensile load. The results showed that incorporating SAP into UHPC enhances the elastic modulus, flexural strength, and tensile strength. Also, mixes with SAP have exhibited compressive strength above 120 MPa after 90 days. Furthermore, the load recovery of the prisms under repetitive flexural load and prisms under sustained tensile loading demonstrated the self-healing efficiency of SAP incorporated into the UHPC mixes higher than the control mix specimens.

Keywords: cracks; self-healing; superabsorbent polymer; ultra-high-performance concrete; sustained loadings; mechanical properties; UHPC



Citation: Alameri, M.; Mohamed Ali, M.S.; Elchalakani, M.; Sheikh, A.; Fan, R. Self-Healing and Mechanical Behaviour of Fibre-Reinforced Ultra-High-Performance Concrete Incorporating Superabsorbent Polymer Under Repeated and Sustained Loadings. *Fibers* **2024**, *12*, 95. <https://doi.org/10.3390/fib12110095>

Academic Editor: Luciano Ombres

Received: 28 August 2024

Revised: 14 October 2024

Accepted: 28 October 2024

Published: 5 November 2024



Copyright: © 2024 by the authors. Licensee MDPI, Basel, Switzerland. This article is an open access article distributed under the terms and conditions of the Creative Commons Attribution (CC BY) license (<https://creativecommons.org/licenses/by/4.0/>).

1. Introduction

Ultra-high-performance concrete (UHPC) exhibits excellent ductile characteristics, primarily due to the strain-hardening behaviour provided by steel fibres in the post-cracking stage under tensile loads. It also possesses remarkable mechanical, ductile, and durability features [1,2]. UHPC is widely applied in numerous construction projects, including concrete bridges and offshore towers [3,4]. However, the production of UHPC requires a low water-to-binder ratio (w/b) of up to 0.2. Consequently, a significant amount of unhydrated cement remains within the UHPC matrix, attributed to the limited availability of water for complete hydration [5]. This low w/b ratio is also responsible for high autogenous shrinkage, leading to the development of microcracks [6]. These cracks affect the internal matrix configuration of the concrete and, as they widen due to shrinkage and applied loads, increase the concrete's permeability to aggressive chemicals accelerating concrete deterioration [7]. In response, many codes of practice such as ACI 224R-01 [8], have stipulated crack width limits, especially for elements exposed to alternating wetting and drying cycles.

In light of these challenges, regular inspection, repair, and maintenance become crucial to ensure the durability and extend the serviceable life of existing concrete structures. Given

the tedious and costly nature of these processes, there is a growing need to develop in-built repair techniques that involve autogenous healing and closing of cracks by incorporating suitable self-healing agents. For example, nanoclay can be used to release water and hydrate anhydrous cement particles [9]. Additionally, other materials like ground granulated blast furnace slag (GGBS) and fly ash are known to promote the hydration process through the emerging carbonation of calcium hydroxide ($\text{Ca}(\text{OH})_2$). Consequently, these innovations enable the healing and sealing of cracks up to 0.1 mm in width [10–12].

Additionally, other healing agents can be utilised to prevent crack formation due to enhanced autogenous shrinkage. These agents function by reserving water and then releasing it later to internally cure the specimens when cracks occur. Lightweight aggregate (LWA), capable of absorbing between 5% and 25% of its weight in water, can significantly boost the internal curing mechanism. This effectively reduces autogenous shrinkage when the internal relative humidity (IRH) reaches around 96% [13,14]. However, an even more effective method of enhancing the healing mechanism involves incorporating a water-absorbing agent into the concrete mix, such as superabsorbent polymer (SAP), which can absorb water up to 1000 times its volume. The efficacy of SAP as an internal curing agent was investigated by Liu et al. [15], where it was found that SAP particles release water to prevent self-desiccation and enhance the hydration process [16,17]. Therefore, by adding SAP to the mix, the autogenous shrinkage of low w/b ratio mixes decreases and the formation of cracks can be effectively detained.

Superabsorbent polymers (SAPs) have been extensively investigated for their capacity to heal cracks caused by applied loads, as reported in numerous studies. In normal strength concrete (NSC), it was observed that cracks up to 0.3 mm could be sealed by using SAP, although this was associated with a notable decrease in the compressive strength of concrete [18,19]. This decrease occurs because SAP particles, after releasing water to promote the self-healing mechanism, leave behind voids [20]. Furthermore, the self-healing mechanism in high-strength concrete (HSC) with compressive strengths up to 100 MPa, particularly in specimens with added SAP has been examined by Olawuyi [21] indicating that the amount of SAP used in the concrete mix significantly affects mechanical properties, such as a reduction in compressive strength by more than 25% due to the presence of voids caused by SAP. Consequently, subsequent studies by Pourjavadi et al. [22], Savva and Petrou [23], and Kang et al. [24] focused on optimising the SAP dosage to achieve an ideal mix. These investigations revealed that a SAP-to-binder ratio ranging from 0.1% to a maximum of 1% provides an effective balance between maintaining mechanical properties and the healing efficiency of the SAP particles.

Recent investigations primarily concentrated on how SAP influences key properties of UHPC, such as shrinkage [15] and tensile strength [25]. The addition of SAP has been shown to significantly alter the shrinkage characteristics of UHPC, which is crucial for minimising crack formation and ensuring structural integrity [15]. Moreover, the effect of SAP on the tensile strength of UHPC was thoroughly explored, revealing insights into how these polymers can enhance the overall mechanical performance of concrete [26]. This body of research contributes substantially to the development of self-healing UHPC with SAPs, making it a more versatile and robust material for modern construction needs.

Cracking the concrete under tension is inherently difficult as it is brittle which could lead to an immediate failure of the specimens hence compressive tests are performed to initiate cracks; in recent studies, it was observed that the cracks occurred in the interfacial transition zone (ITZ) at around 70% of the compressive strength of the cubes [27–30]. However, adding the steel fibre to the concrete matrix can enhance the ductility and allow the specimens to be cracked in the tension face such as under three- and four-bending tests [31–34], direct tensile strength [35,36], and splitting tensile strength tests [37,38]. Repetitive loads were also introduced to create cracks and evaluate the self-healing mechanism [39–41].

The primary objective of this study was to conduct a comprehensive investigation into the influence of SAP on the mechanical properties of UHPC. Given the limited experimental data available, this research aimed to explain the self-healing mechanisms of UHPC

when incorporating a small amount of SAP, whereas previous studies have proved that adding above 1% of SAP will rapidly deteriorate the mechanical performance of concrete. Furthermore, a direct correlation between the microstructural modifications and the macro-behaviour of UHPC mixes was established, both with and without SAP inclusion, to gain deeper insights into how these variations affect the overall performance of the material. A distinctive aspect of this study involved subjecting UHPC specimens containing SAP to sustained tensile loading for a duration of 28 days, providing a novel approach to assess the healing ability of these materials under continuous stress conditions. By addressing these objectives, this study aimed to contribute significantly to the development of self-healing UHPC, enhancing its versatility and robustness for contemporary construction applications.

2. Experimental Programme

The full experimental programme is illustrated in Figure 1. Three different mixes produced for the purpose of comprehensively evaluating the mechanical performance, durability characteristics, microstructural analysis, and self-healing capabilities under different curing conditions represent the most common curing conditions in real-world scenarios without considering the aggressive conditions.

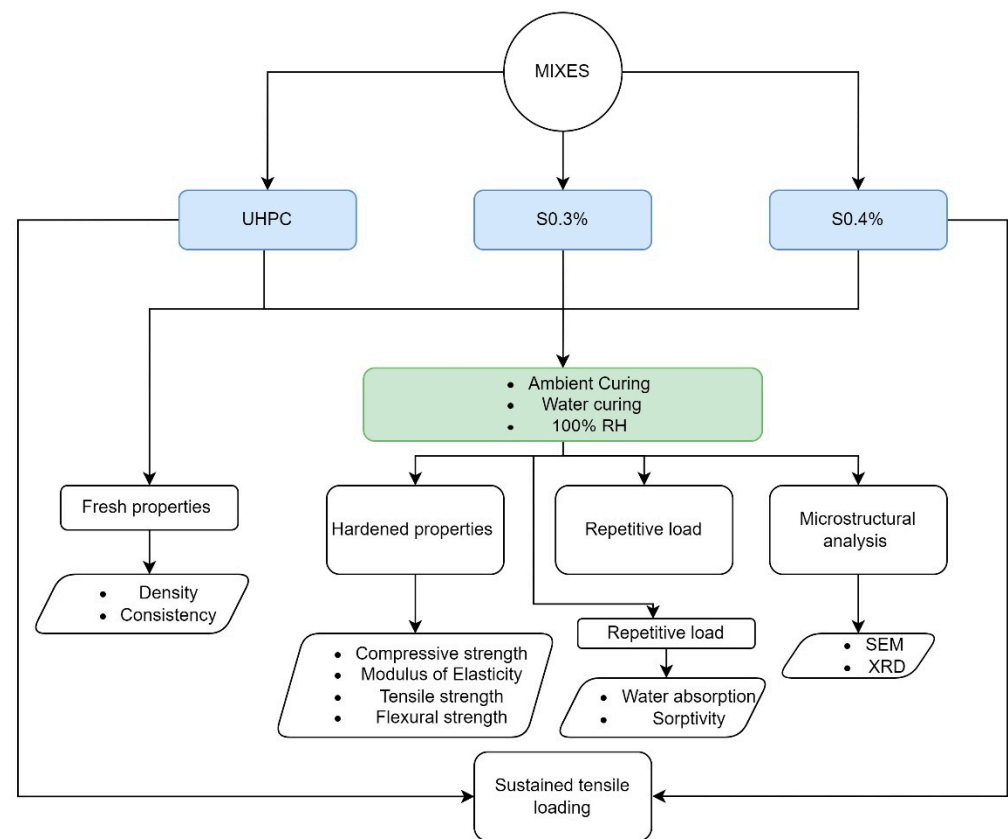


Figure 1. Flow chart of the experimental programme.

2.1. Material Used

The two main binders of this study were Portland cement and ground granulated blast furnace slag (GGBS); silica fume was used as a supplementary binder. The chemical compositions for the binders are summarised in Table 1. Blended and dried sand with high silica contents, sub-angular to rounded grains, and a diameter size ranging from 0.075 mm to 1.18 mm were utilised as fine aggregate. High-range water reducer (HRWR) with 36% solid contents by mass (polycarboxylates superplasticiser (SP), ViscoCrete-10 type, Sika, Sydney, Australia) was used to enhance the workability of the mix. High-strength microsteel fibre with a diameter of 0.2 mm and length of 13 mm with a tensile

strength of 2500 MPa was utilised for ductility. The SAP type used in the mix is called Polyacrylate/Polyalcohol Copolymer with a variation in the diameter size between 0.05 mm to 0.5 mm, which can absorb up to 60 g/g.

Table 1. Chemical composition by mass %.

Materials	SiO ₂	TiO ₂	Al ₂ O ₃	Fe ₂ O ₃	MgO	CaO	Na ₂ O	K ₂ O	P ₂ O ₅	SO ₃
Cement	19.51	0.26	5.03	2.86	1.59	61.44	0.19	0.37	0.06	2.14
GGBS	35.10	0.57	13.59	0.98	5.36	41.52	0.14	0.33	0.04	0.10
SF	92.35	0.01	0.36	0.78	0.36	0.54	0.19	0.52	0.31	0.04
Quartz sand	93.48	0.04	0.06	0.06	0.03	0.02	0.039	0.02	0.01	0.01

2.2. Mix Proportion and Curing

2.2.1. Mix Procedures

The mixture details of UHPC are summarised in Table 2. The binder consists of OPC and GGBS only where (s/b) represents the fine aggregate-to-binder ratio and w/b represents the water-to-binder ratio, and SAP (%) and SP (%) refer to the percentage of the binder. UHPC denotes the control mix without added SAP, whereas S0.3 and S0.4 denote the concrete mix with a SAP dosage of 0.3% and 0.4% of the binder ratio. Initially, trial mixes with varying water and SP contents were carried out to optimise the workability of the wet mix so that it can be used in the further full-scale batches of the mix. For the mixing procedure, the dry cementitious materials (OPC, GGBS, and SF), sand, and SAP were mixed at room temperature for three minutes. Then, 90% of the water was added for one minute, followed by the SP mixed with the rest of the water and added to the mix. After that, the wet mixing was continued until the desired consistency was obtained. Finally, the steel fibre was added to the mix for another three minutes to distribute the fibres homogeneously to the mix. Note that the mixing time can vary from the mixes due to the effect of added SAP dosages.

Table 2. Mix proportions.

Mix ID	Binder (%)		Silica Fume (%)	s/b	w/b	* Added Water/b	SAP (%)	Steel Fibre (%) (Volume Fraction)	SP (%)
	Cement	GGBS							
UHPC	85	15	25	1.1	0.166	0	0	1.5	4
S0.3						0.0129	0.3		
S0.4						0.0172	0.4		

* The additional water needed to address the absorption of the SAP is calculated based on the SAP's absorption rate.

2.2.2. Curing

The fresh mix was poured into different moulds (cubes, cylinders, and prisms) and then these were cured under three different curing regimes namely: (i) ambient curing in the constant temperature chambers with 25 °C and 50% relative humidity (RH); (ii) water curing in ambient room temperature and humidity conditions; and (iii) 100% RH curing in a fog room. The specimens were demoulded after 24 h; curing commenced immediately and the specimens were cured under the prescribed curing regimes until the day of testing. In the case of reloading experiments, where the prisms were tested under the load again after 28 days, they were placed under the same curing condition after the initial loading stage.

2.3. Methods

2.3.1. Fresh Properties

The consistency test of all fresh mixes was conducted according to ASTM C1437 [42]. The unit weight of fresh concrete was obtained immediately after preparing the mixture by using a cylindrical mould.

2.3.2. Hardened Concrete

An MTS 300 kN closed loop Servo control testing machine with a data acquisition system was used for the flexural and tensile strength tests. After 28 and 56 days, the flexural strength test was conducted by testing a prismatic specimen (100 mm wide, 100 mm deep, and 500 mm long). The applied load was controlled by using a displacement rate of 0.1 mm/min.

In order to evaluate the tensile strength of the mix, dog bone specimens were prepared as shown in Figure 2, according to the details provided by Singh et al. [43]. The concept of this specimen was to provide two gripping portions at the top and bottom and a shank in the middle. The gripping portions were large enough, which were half the length of the shank, to prevent any premature failure that could happen due to insufficient area. The gripping portions were designed to gradually decrease the width to match the width of the shank. Therefore, the purpose of this test was achieved by failing the specimen in the shank area. Hence, four linear variable differential transformers (LVDTs) (two on each side) were attached to the shank of the specimen to measure the strain and the crack opening. A very low displacement rate control of 0.002 mm/min was utilised to gradually apply the load and ensure that there was no quick and sudden failure in the specimen.

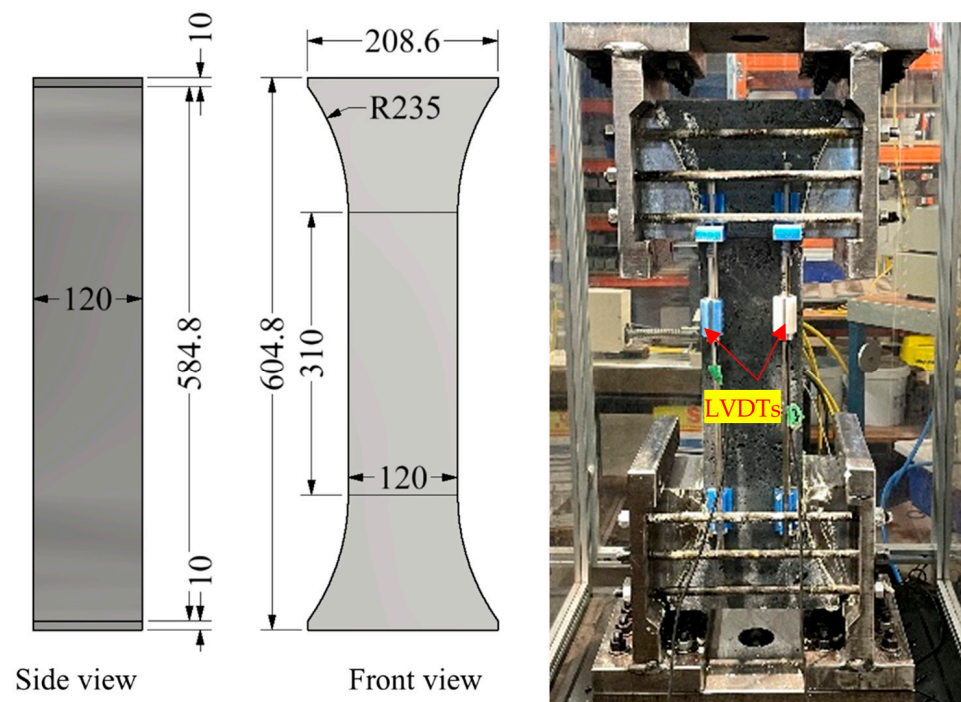


Figure 2. A diagrammatic view of dog bone test and the set-up under uniaxial tensile loading (dimensions in mm).

The compressive strength and the modulus of elasticity of the concrete were evaluated using cylindrical specimens (100 mm diameter \times 200 mm height) according to the ASTM C39 [44]. The modulus of elasticity test was conducted by bonding four strain gauges to the specimens at their mid-height (two in the longitudinal direction and two in the transverse direction). Moreover, LVDTs were also used on opposite sides to confirm the readings from the axial strain gauges.

2.3.3. Durability Properties

Three-disc specimens each with a diameter of 100 mm and a height of 50 mm were cut from a cylindrical specimen to evaluate the effective permeable porosity of each mix according to the guidelines of ASTM C642 [45]. To achieve a constant mass, the specimens were placed in the oven to be dried for 24 h at a temperature of 110 °C. Then, the initial

weight (w_i) was measured after placing the specimens at room temperature (25 ± 1 °C); they were then submerged in water for four days to obtain the saturated weight (w_s). The water absorption was calculated by using Equation (1).

$$\text{Water absorption, \%} = \left(\frac{w_s - w_i}{w_i} \right) \times 100 \quad (1)$$

The sorptivity is an important feature in evaluating the water absorption and transmission via the capillary action of the concrete. The sorptivity test was conducted according to the guidelines of ASTM C1585 [46]. Three cylindrical specimens with a diameter of 100 mm and height of 50 mm were cut from the 28 day-cured cylinder for each mix. The specimens were placed in the oven to be dried for three days at a temperature of 50 °C. Afterwards, the specimens were left at room temperature (25 ± 1 °C) for 24 h to cool down. Subsequently, they were put in a storage container and left again at room temperature for 15 days. A waterproof tape was used to cover all the peripheral surfaces except the bottom surface to protect the specimens from any flow of water. The base of the specimens was then drowned with a level of water around 3 mm. The specimens were then measured at different intervals up to 8 days. The sorptivity was thus evaluated according to Equation (2).

$$S = \frac{I}{t^{1/2}} \quad (2)$$

where t is the time-lapse in minutes, and I can be calculated from Equation (3) which is the cumulative water absorption (per unit area of inflow surface, mm).

$$I = \frac{\Delta m_t}{a \times d} \quad (3)$$

where Δm_t is the change in mass with time t in grams, a is the exposed area in mm² of the specimen, and d is the density of water in g/mm³.

2.3.4. Load Recovery Under 3-Point Bending Test

It is well-established that the UHPC mainly develops microcracks due to its dense matrix [47]. To effectively quantify and control these cracks, two specific indicators were employed to induce cracking in the specimens. The displacement ratio of the flexural strength test was measured prior to conducting the test at approximately 85% of the expected flexural displacement, the test was intentionally halted and the specimens were returned to their initial curing regime for an additional 28 days. Moreover, post-initial crack formation, each specimen was closely monitored to pre-empt any unforeseen failures. Notably, the presence of steel fibres in UHPC may manifest as curve fluctuations in the observed crack patterns due to the effect of the addition of steel fibres in the mix.

Two specimens were tested to evaluate the self-healing mechanism under repetitive loading. Details of the first specimen along with the testing setup are illustrated in Figure 3. For precise crack detection, a Crack Mouth Opening Displacement (CMOD) was employed across a notch in this specimen and continuously monitored at a rate of 0.1 mm/min. CMOD was utilised to measure the opening of the cracks inside the notched specimens. The second specimen was unnotched and it was tested similarly to the notched specimen without any CMOD measurement.

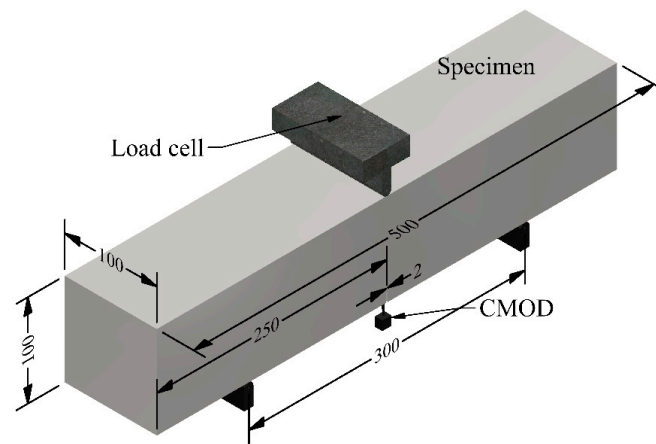


Figure 3. Notched specimens (dimensions in mm).

2.3.5. Microstructural Observations

Backscattered electron (BSE) imaging was utilised to assess the compactness of UHPC with and without SAP particles. The impact of SAP particles on the density of the microstructure including the interfacial transition zone (ITZ) was examined. The healing product and the matrix of the UHPC were also performed at specific points on the samples using energy-dispersive X-ray spectroscopy (EDX). For this, samples were collected from -thenotched specimens after the second loading stage. To halt further cement hydration, these samples were submerged in ethanol alcohol for three days and then oven-dried for an additional three days to ensure complete dryness. Moreover, each sample was enclosed in epoxy resin to create a stable mould and subsequently polished with sandpaper to prepare them for the experiment.

Additionally X-ray diffraction (XRD) analysis was conducted to quantify mineral phases in the mixes. Freshly broken samples were taken from the flexural strength test after 28 days and the notched pre-cracked specimens after 56 days of curing. These samples were ground and prepared for the experiment. The ambient curing samples from all mixes were selected to be the representative samples in this experiment. It can be argued that ambient curing simulates realistically the condition in the internal parts of concrete elements. XRD patterns were recorded with a PANalytical X'Pert Pro Multi-purpose Diffractometer using Fe-filtered Co K α radiation, an automatic divergence slit, 2 $^\circ$ anti-scatter slit, and fast X'Celerator Si strip detector. The diffraction patterns were recorded in steps of 0.017 $^\circ$ 2 θ with a 0.5 s counting time per step for an overall counting time of approximately 30 min. Qualitative analysis was performed on the XRD data using in-house XPLOT and High-Score Plus (from PANalytical, Malvern, UK) search/match software. Furthermore, quantitative analysis was performed on the XRD data using the TOPAS version 6 Rietveld analysis software (from Bruker AXS, Melbourne, Australia).

2.3.6. Prisms Under Sustained Loading

Prismatic specimens with a cross-section of 75 mm \times 75 mm and a length of 500 mm were poured and then cured for 28 days under ambient curing conditions. The test set-up is presented in Figure 4 for preparing and testing these specimens. The specimens were kept under sustained tensile loading for 28 days. At the mid-height of the specimen, a groove was made to measure the crack initiated by the applied tensile load. The cracking load was applied for 28 days under wet and dry curing cycles of two days where conditions were continuously altered. A water holder was designed specifically for this experiment to cure the area that cracked. For the purposes of the measurement, two LVDTs were attached on each side near the mid-height of the specimens. Moreover, a strain gauge was bonded to the threaded rod for the purpose of measuring the induced stress in the specimens. These strain values were converted to the equivalent stresses or loads according to the material properties of the threaded rod.

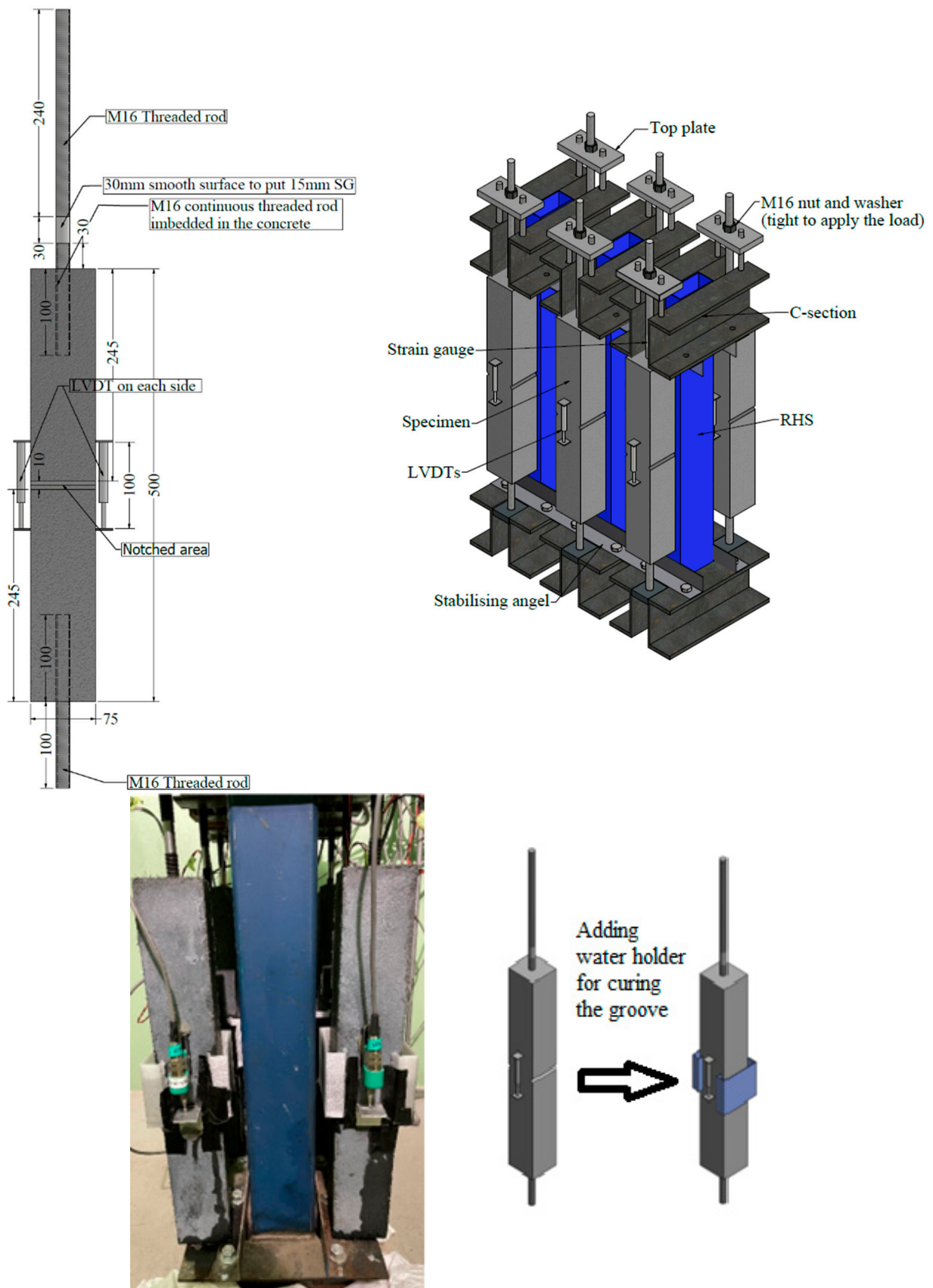


Figure 4. Test set-up of specimens under constant loading (dimensions in mm).

Initially, the specimens were subjected to a steadily increasing applied load until the first crack existed and then it was lowered to 50%, 60%, or 70% of the maximum load according to the results from the tensile strength tests; these reduced loads were sustained for a different period of days. The loads were adjusted manually to avoid any potential premature failure. Table 3 shows the different levels of loads and stresses that have been extracted from the tension test of the threaded rod.

Table 3. Stresses and loads under tensile strength.

	UHPC	S0.4
Stress at First crack (MPa)	4.50	3.84
Max. Stress (MPa)	4.62	4.14
Equivalent load for max stress (kN)	24.26	21.74

3. Results and Discussion

3.1. Fresh Properties

Commercially available SAP was procured from a single source in Australia and was mixed in its dry condition without any specific treatment. However, the effect of SAP dosages and w/b ratio on density and consistency of the fresh concrete was investigated in this study. Density is an important indicator of the strength and durability of hardened concrete, whereas consistency improves compatibility consolidation and ease of placement.

Figure 5 illustrates the properties of the fresh concrete for all mixes. It shows that adding SAP with extra free water resulted in a minor reduction in the density, a decrease of 0.86% for S0.3 and 1.15% for S0.4 from the corresponding UHPC control mix. This was due to the absorption of water by SAP during the mixing process as SAP can absorb up to 60 g/g. However, adding extra water to adjust for the water absorbed by SAP to maintain the consistency did not enhance the consistency as can be seen in Figure 5. Note that the control mix had 35% of consistency whereas the mixes S0.3 and S0.4 had a consistency of 33% and 37%, respectively. The main factor for changing the consistency of each mix was the ability of SAP to absorb the water in the slurry, as reported previously [48].

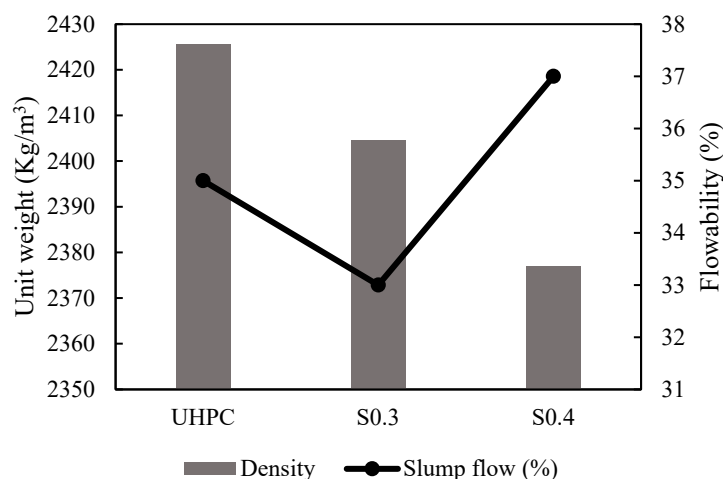


Figure 5. Fresh unit weight and consistency results.

3.2. Hardened Properties

3.2.1. Compressive Strength and Elasticity

Figure 6 presents the compressive strength for all mixes at different time intervals (7, 28, 56, and 90 days) with varying conditions of curing (ambient, water, and 100% RH). UHPC mix with ambient curing had the highest values across all ages. Note that when correlated with the density results shown in Figure 7, the ambient-cured specimens exhibited higher compressive strength values across all ages as the denser the concrete,

the better the behaviour under compression. Also, the compressive strength decreased with the increase in SAP dosages, specifically at the early stages. After seven days, the ambient curing mix without SAP had a higher value than S0.3 and S0.4 by 28.8% and 37.3%, respectively. Furthermore, a similar trend was observed for both water-cured and 100% RH curing specimens. For instance, in the case of water curing, the decrease in compressive strength was 12.5% for S0.3 and 21.2% for S0.4 compared to the corresponding control specimens. It can also be seen from Figure 6 that the compressive strength increased gradually with time in all mixes with different curing conditions. At 28 days, the ambient-cured control specimen had the highest value, whereas the water-cured specimens yielded the best values for UHPC mixes with SAP; the difference between the control mix and S0.3 was 5.9% whilst it was 6.8% for mix S0.4.

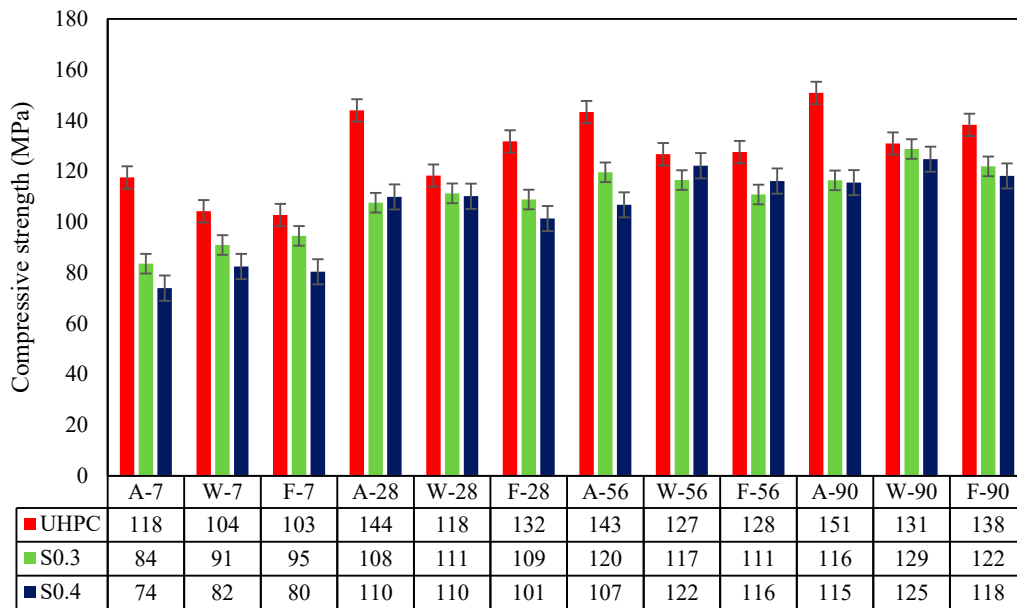


Figure 6. Compressive strength for 7, 28, 56, and 90 days for all mixes and different curing conditions (A = ambient, W = water, F = 100% RH).

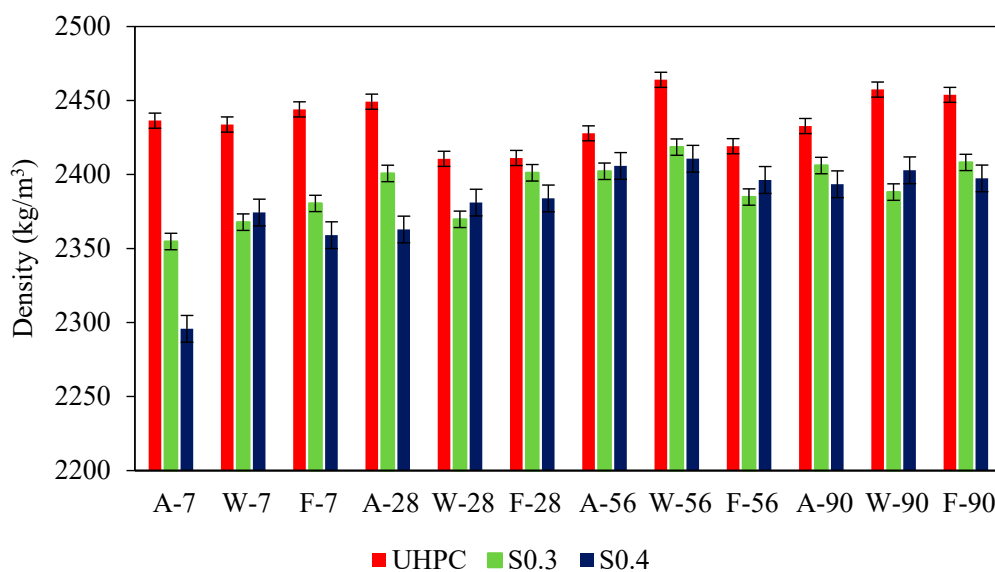


Figure 7. Density at 7, 28, 56, and 90 days for all mixes with different curing conditions (A = ambient, W = water, F = 100% RH).

Further decline of the difference in compressive strength between UHPC with and without SAP was noticed at 90 days; for example, for mix S0.3, the difference was 1.5% which was negligible. This proved that SAP efficiently assisted in the further hydration of the anhydrous cement particles with the increase in age [49]. On the other hand, the decrease in compressive strength was caused by the voids made by SAP after the desorption of water [50].

Table 4 summarises the modulus of elasticity values for the water-cured specimens at 7 and 28 days along with the corresponding maximum strain. Overall, the specimens with SAP exhibited higher stiffness than the control specimens without SAP. This was in contrast to the compressive strength results, as the modulus of elasticity of S0.3 at 7 days and 28 days showed an increase of 8.7% approximately. Therefore, it can be stated that adding SAP leads to improved modulus of elasticity as adding SAP causes the closure of microcracks and hence the stiffness of the concrete [51].

Table 4. Modulus of elasticity for all mixes for water curing on 7 and 28 days alongside the related mechanical properties, water absorption, and volume of permeable voids.

Mix ID	No. of Days	E_c (GPa)	Max. Stress (MPa)	Max. Strain ($\mu\epsilon$)	Water Absorption (%)	Volume of Permeable Voids (%)
UHPC	7	42.4	108.00	3173	1.34	3.24
	28	46.2	125.79	2938		
S0.3	7	46.3	95.71	2892	2.38	5.46
	28	50.6	118.45	2818		
S0.4	7	48.4	82.97	2385	2.51	5.47
	28	47.4	112.40	2830		

3.2.2. Flexural and Tensile Strength

Figure 8 shows the flexural strength results of all mixes after 28 days and 56 days. For 28 days, S0.3 under water curing had the best results with a flexural strength of 23.46 MPa whilst for the control mix, the best results were recorded for the water-cured specimens. Contrary to the previous results at 28 days, S0.4 had the highest value of flexural strength under 100% RH with 19.65 MPa. For 56 days, the flexural strength of S0.3 was slightly decreased under water curing. However, improved results were observed for ambient and 100% RH curing mixes. For UHPC without SAP, a minor decrease in the flexural strength for the water curing and almost no reduction in strength for the ambient curing was observed. It is interesting to note an increase of 29.7% for the 100% RH-cured specimen. For S0.4, the results fluctuated between an increase in water and ambient curing and a decrease in the 100% RH curing conditions. The failure of all specimens occurred due to the extensive formation of microcracks; the steel fibres influenced this behaviour as they bridged the cracks, which yielded better strength. Hence, for flexural strength, a combination of SAP and fibre led to better performance of UHPC with SAP which was contrary to the compressive strength behaviour as SAP prevented self-desiccation which decreased internal relative humidity [52]. Consequently, the microcracks could be limited in the mixes with SAP.

The stress/strain relationship under the tensile load for all mixes under ambient curing is shown in Figure 9. The behaviour of specimens under direct tensile load can be classified into three levels: (i) the elastic region with the influence of fibre; (ii) the strain hardening region where the curves fluctuate at the peak strength due to the presence of steel fibres with an increase in the strain; and (iii) the strain softening process. Additionally, the fibre bridging behaviour affects the behaviour regardless of the effect of adding SAP. The SAP effect peaked with S0.3 with elastic behaviour until the peak stress. However, a drop of about 21.5% in the strength happened immediately after the peak stress, which transformed the curve to be in the strain hardening region with another drop to start the softening of the specimen after reaching above 4000 $\mu\epsilon$. Alternatively, UHPC control and S0.4 specimens

had lower strength but exhibited similar behaviour throughout. Interestingly, the S0.4 had the best strain hardening behaviour among the specimens and at around $6000 \mu\epsilon$, it held a higher load. However, a rapid decline in S0.4 happened, whereas the other specimens had a consistent decline. As mentioned previously in the flexural strength behaviour, the benefit of SAP to prevent self-desiccation, which increases the internal curing along with crack-bridging due to steel fibres to bridge the crack, helps in explaining the results of tensile strength. Similar findings have been found in a previous study by Assmann and Reinhardt [53].

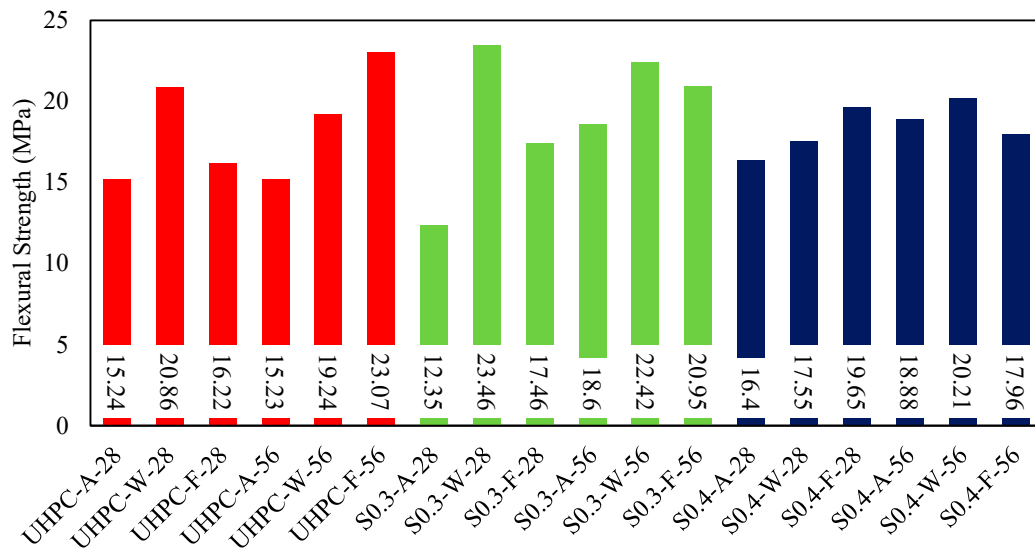


Figure 8. Flexural strength for all mixes at 28 and 56 days with different curing conditions.

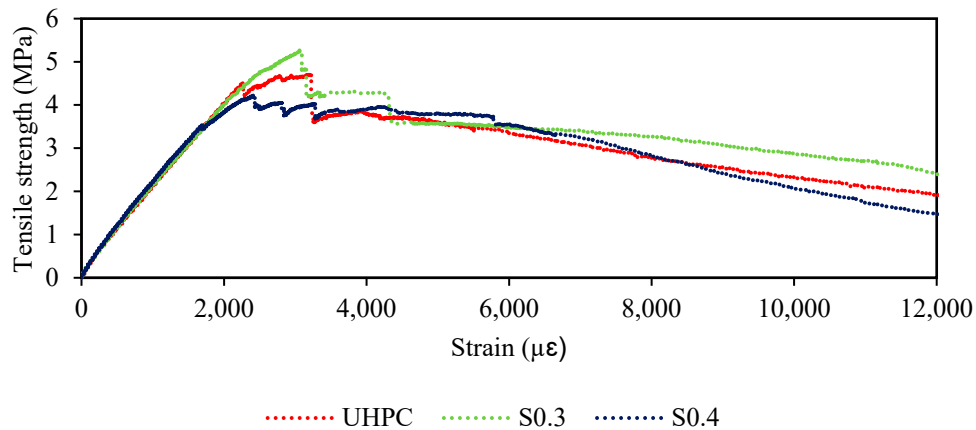


Figure 9. Stress/strain curve for tensile strength for all mixes under ambient curing condition.

3.3. Mechanism of Self-Healing

The healing mechanism could be understood by applying the flexural load repetitively; for this, the load was initially applied to initiate the cracks and then the specimen was unloaded to subject it to a specific curing condition for a desired age. Figure 10 illustrates the load/CMOD relationship under the three points bending test under different curing regimes. The cracks were initiated by the application of the load. After unloading, the specimens were subjected to the same curing condition for 28 days and then the load was reapplied. During the test, the specimen under load was monitored carefully to prevent premature failure as in some specimens, the crack opening did not attain the desired value for the purpose of this healing study (0.2 mm measured via CMOD). The results of ambient-cured specimens showed that S0.3 and S0.4 had a higher capacity for load recovery after 28 days than the corresponding control specimens. For water-cured

specimens, similar behaviour was also observed which confirmed the results found by Qian et al. [54]. Qian et al. found that the recovery of water-cured specimens reached about 105% of the original load. On the contrary, specimens under 100% RH curing showed comparable results between the UHPC control mix and S0.3. However, the S0.4 mix exhibited better performance in terms of load recovery. Hence, it can be concluded that the restoration of load under different curing regimes and healing capacity were maintained by adding SAP.

Figure 11 presents the load recovery after the first loading and reloading after 28 days. It can be clearly stated that the UHPC mixed with SAP performed better in the reloading process. UHPC without SAP also increased the stress capacity after the first load. The reason behind this recovery of load for UHPC could be related to two different components: (i) the steel fibre could bridge the crack [51], and (ii) blast furnace slag can limit the crack and improve its durability [55].

Furthermore, calcite formation in the cracks was noticed immediately after applying the load for water-cured specimens of S0.3 as shown in Figure 12. This observation signifies the self-healing mechanism due to the presence of SAP particles. The internal curing provided by SAP enhanced the hydration products in the concrete matrix by realising the water that formed $\text{Ca}(\text{OH})_2$ internally and reacted with carbon dioxide externally to form the calcium carbonate (CaCO_3), which is called calcite, to heal the crack efficiently [56].

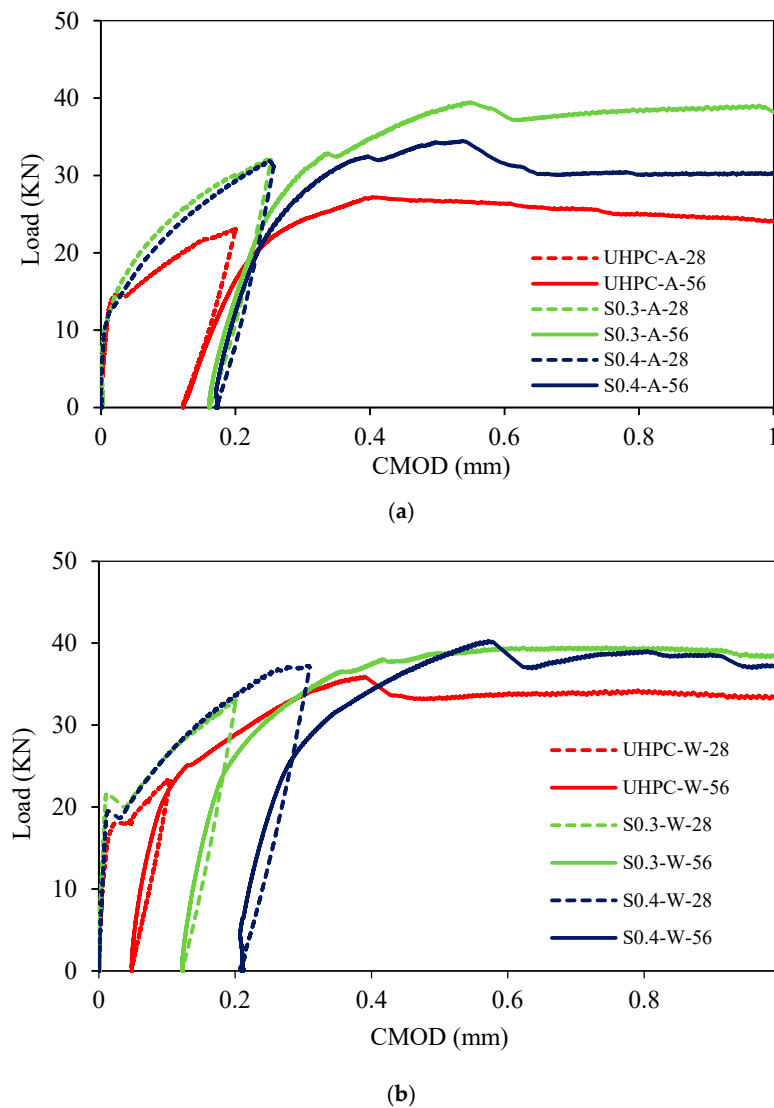
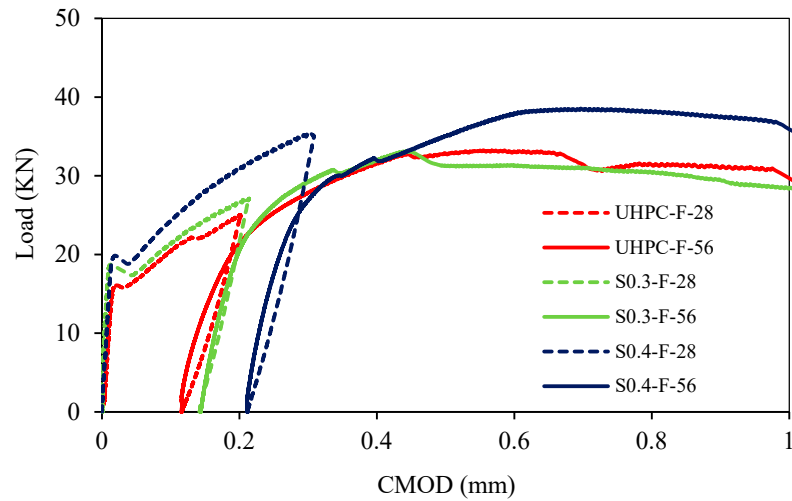


Figure 10. Cont.



(c)

Figure 10. Load/CMOD relationship after applied loading until up to 0.2 mm, then reloading after 28 days from the first loading applied. (a) Ambient curing; (b) water curing; and (c) 100% RH curing.

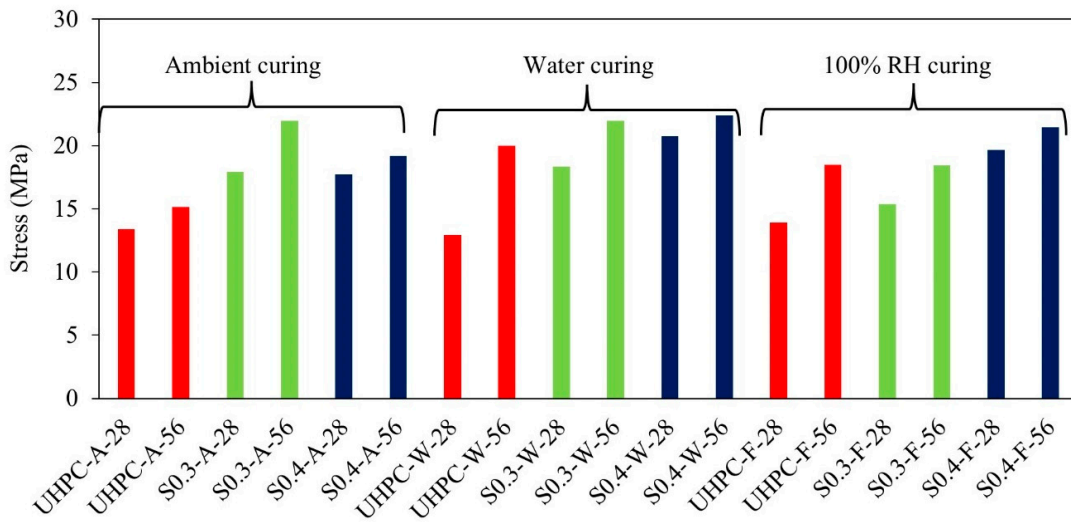


Figure 11. Load recovery for all mixes under different curing conditions.



Figure 12. Formation of calcite immediately after the cracking load of 28 days (S0.3 with water curing).

3.4. Durability Characteristics

Table 4 shows the results for water absorption and porosity by indicating the volume of permeable voids after 28 days for all mixes. It can be seen that the water absorption was higher in the mixes with SAP and increased with the increased SAP dosages as SAP increased the porosity of UHPC and it was observed by Zhutovsky and Kovler [57] that the very low w/b ratio also involved in this process could increase the porosity.

The absorption rate and sorptivity results are illustrated in Figure 13 which reveals the mechanism of water migration through concrete and the absorption rate of the UHPC control mix had a lower rate among the mixes. This finding correlates well with the results of compressive strength, where UHPC had the highest values regardless of the curing condition. It could be attributed to the capillary mechanism of UHPC, which prevents water movement within the concrete. For both S0.3 and S0.4, the absorption rate was almost similar whilst the results of sorptivity indicated that the initial absorption was higher with the increase in SAP dosages. On the other hand, the sorptivity attained similar values for all mixes with time. Therefore, it is evident that the outer layers of the specimens for mixes with SAP effectively absorbed the water and then restrained the movement of water within SAP particles or concrete.

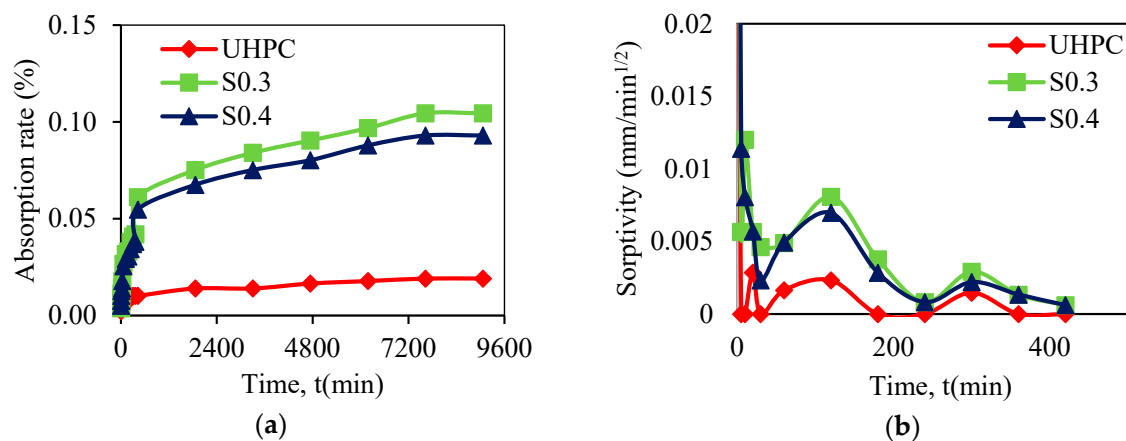


Figure 13. Sorptivity results of all mixes after water curing of 28 days: (a) the water absorption; and (b) sorptivity.

3.5. Microstructure Investigation

For all mixes, BSE images recorded at 56 days are shown in Figure 14. Additionally, EDX for specific points was plotted. The voids indicated by smooth dark spots are clearly visible for the mixes S0.3 and S0.4 due to SAP particles. These voids will disintegrate the concrete matrix which will correspondingly affect the mechanical strength specifically the compressive strength as it can be observed in the compressive strength results. According to the EDX magnification, SAP had a high amount of element C and the product formed around SAP particles was calcium silicate hydrate (C-S-H) gel. Therefore, it is interesting to see the C-S-H as the main product of healing around the SAP particles which shrunk after the desorption of the water that can be extracted from the size of the SAP voids. Independent of the curing regime, the region around SAP particles consists of CaCO_3 and $\text{Ca}(\text{OH})_2$ with a minimal gap which differs from the NSC as mentioned in [58]. Thus, SAP particles densify the microstructure by enhancing the hydration products [51,59]. Evidently, SAP creates voids and weakens the matrix of the UHPC but gradually SAP desorbs water to hydrate the anhydrous cement particles around the voids to make C-S-H gel. Due to the high amount of cementitious materials in the UHPC, SAP yields C-S-H gel as a healing product which was proved to be the best product for the matrix that causes the concrete to gain more strength [60].

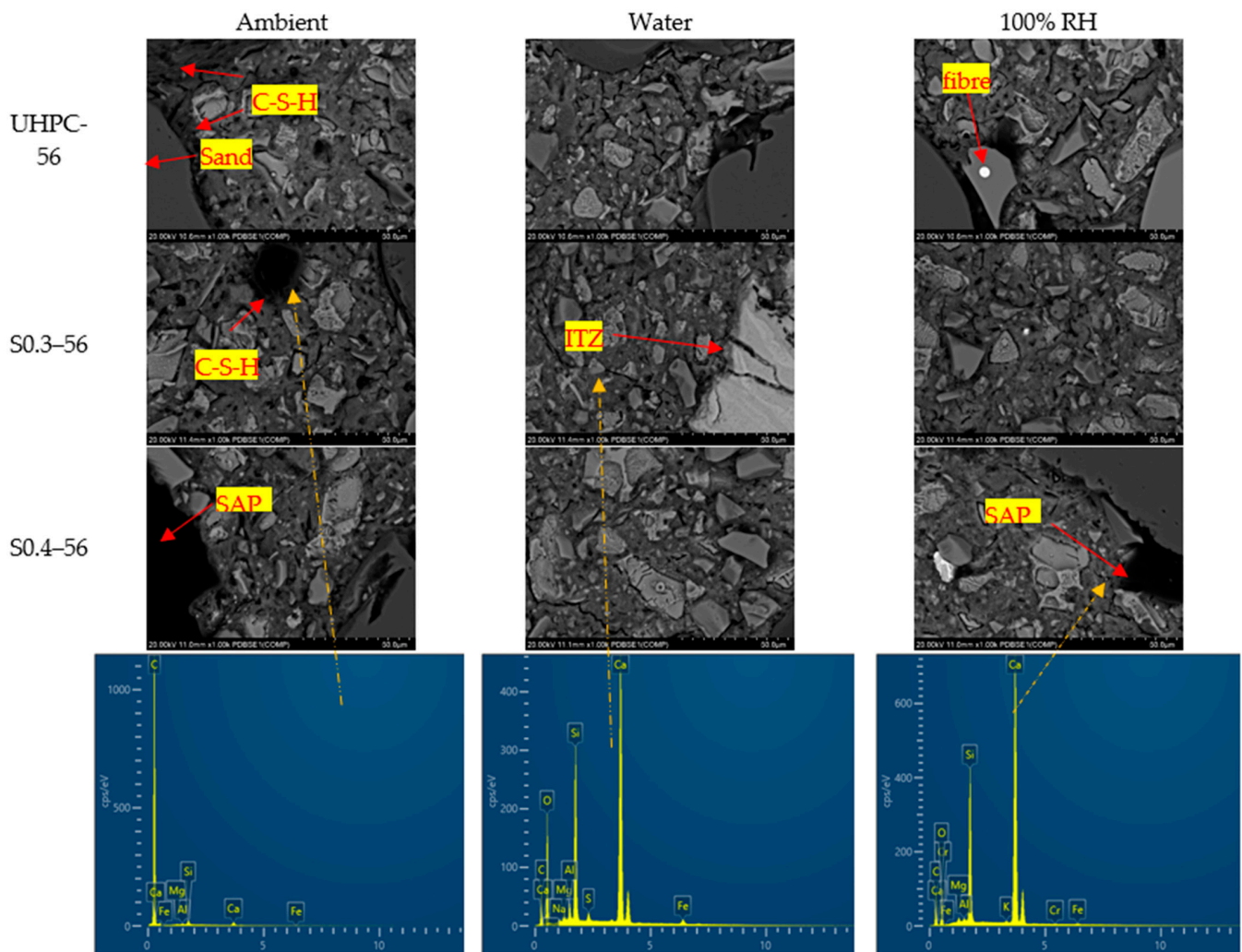


Figure 14. SEM images after 56 days with different curing regimes.

XRD results of the ambient curing of flexural strength test after 28 days and reloaded notched specimens after 56 days are shown in Table 5 and Figure 15. While the amount of SAP differed in each mix, the calculated chemical composition results were very close to each other. However, UHPC-28 days had the highest amount of C_3S composition followed by S0.3-28 and S0.4-28. Therefore, the amount of the hydrated product in mixes with SAP was greater than that without SAP. Calcite forming $CaCO_3$ product for the healing purposes was also reduced in S0.4 by 20%, S0.3 1%, and UHPC 12%. Therefore, S0.4 after 56 days had produced more $CaCO_3$. Ettringite which is responsible for forming the expansion for the matrix, was seen in the quantitative data of mixes with SAP by Bentz and Jensen [61]. Interestingly, ettringite was also traced in the UHPC-56 days in this study. Furthermore, the lower w/b ratio also led to further hydration of the anhydrous particles.

Table 5. Quantitative XRD results of the matrix of mixes (wt.%).

	UHPC-28	UHPC-56	S0.3-28	S0.3-56	S0.4-28	S0.4-56
Portlandite	1.0	0.4	0.7	-	-	-
C_3S	18.9	13.5	16.4	12.9	16.4	13.3
Quartz	63.3	69.1	67.9	70.7	64.2	72.0
Calcite	10.5	9.2	9.8	9.7	11.0	8.8
C_4AF	3.5	2.9	3.1	2.6	3.4	2.4
C_2S	1.8	2.4	1.4	1.5	2.4	0.7
C_3A	1.0	0.8	0.8	0.9	1.0	0.7

Table 5. Cont.

	UHPC-28	UHPC-56	S0.3-28	S0.3-56	S0.4-28	S0.4-56
Ettringite	-	1.8	-	1.8	1.5	1.4
Dolomite	-	-	-	-	-	0.6
SUM (%)	100	100	100	100	100	100

— UHPC-28 - - - UHPC-56 — S0.3-28 - - - S0.3-56 — S0.4-28 - - - S0.4-56

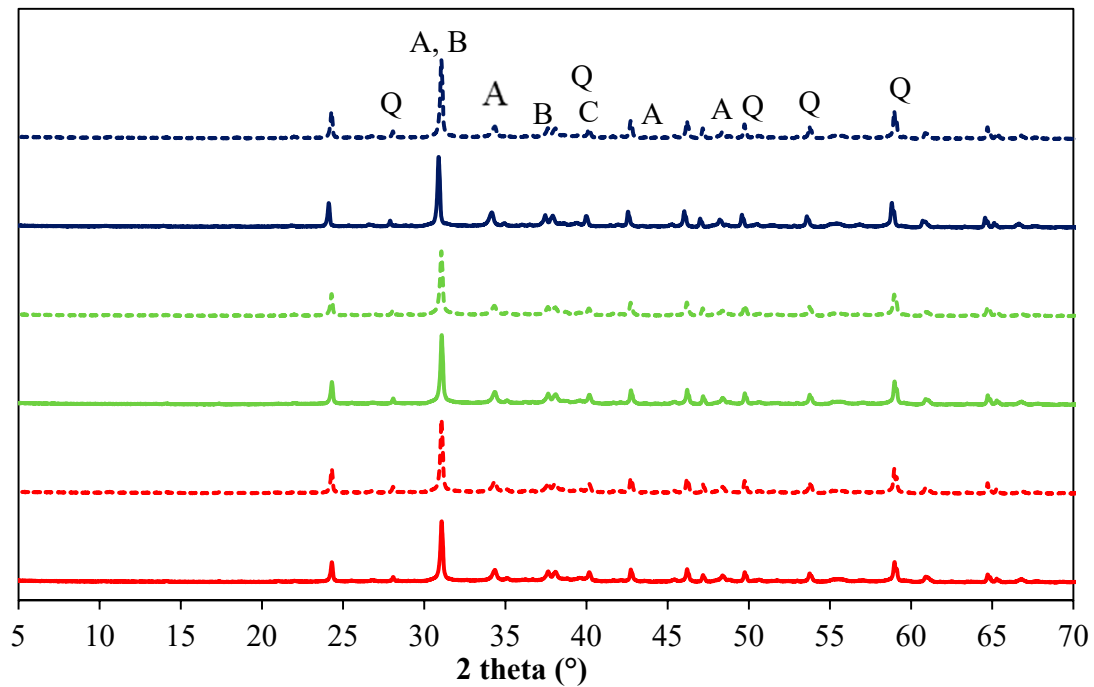


Figure 15. XRD spectra of the mixes after 28 and 56 days [A = alite, B = belite, C = calcite, and Q = quartz].

3.6. Behaviour of the Prisms Under Constant Tensile Load

In Figure 16, the change in the displacement (the opening of the crack at the notched area and average of two LVDTs values) over time is illustrated. For S0.4, the crack in the specimen occurred on day 1 where the stability of the plateau implied there was no dynamic variation in the crack closure. For the UHPC control mix, the crack was triggered on day 9; this is due to the fact that the load was applied slowly to ensure there would not be a premature failure. For all the specimens, the displacement almost remained constant during the whole period except for the UHPC specimen, which raised slightly after day 9. The increase is due to the nature of the load, which was applied periodically to initiate the cracks.

Figure 17 shows the stress throughout the entire test period. The load was applied recurrently to achieve the cracking load. For S0.4, the stress reached around 8 MPa on day 1 and then it was lowered to 2 MPa, which corresponded to 50% of the load that caused the crack based on the results extracted from the tensile strength experiment in Section 3.2.2. The stress was increased cyclically on days 1, 3, 5, 7, and 9. At day 9, the stress remained at 2 MPa for up to 15 days. It is evident that the stress increased autogenously throughout this interval as the healing capability of S0.4 was demonstrated by the surge in stress rather than a reduction in displacement. For the UHPC control specimen, the load was increased on the same days as S0.4 and the crack was initiated on day 9; the load was adjusted on day 12 to reach 50% of the cracking load. For the next 12 days, the load continued constantly, and it was increased at the end of this period, which caused the failure of the specimen,

implying no increase in the capacity of the specimen. Therefore, S0.4 was more effective at healing the cracks and recovering the stiffness at the same displacement reading for both wet and dry cycles.

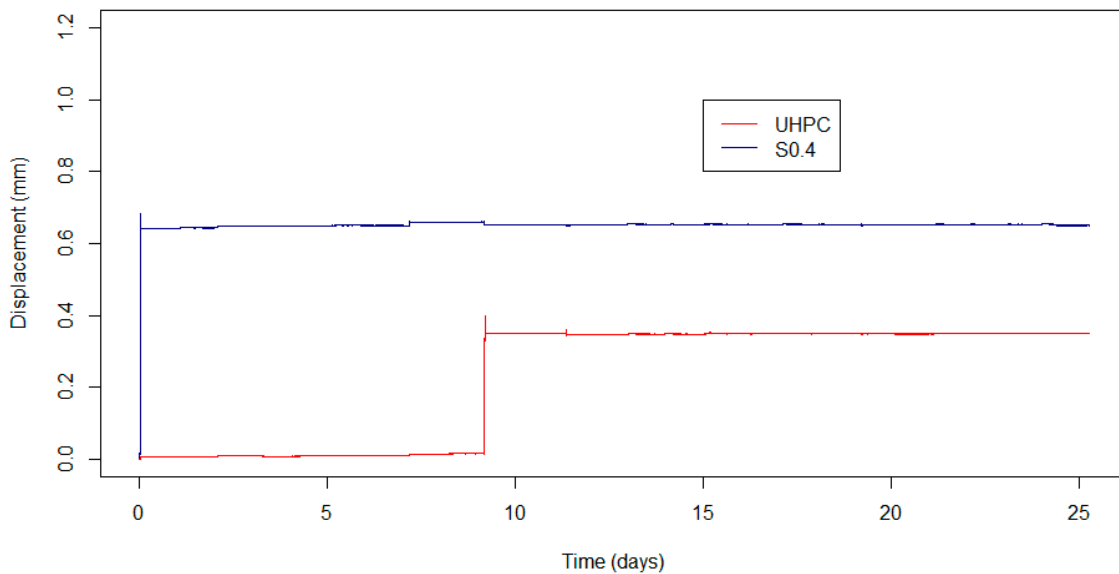


Figure 16. Displacement vs. time for wet and dry cycles.

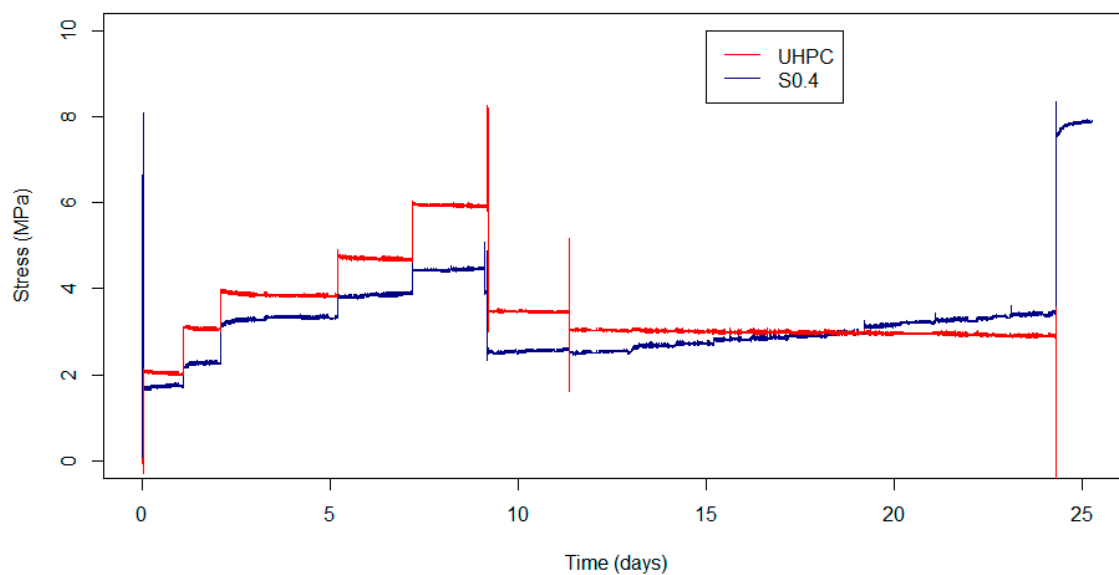


Figure 17. Stress vs. time for wet and dry cycles.

4. Conclusions

This study investigated the effect of incorporating SAP into UHPC mixes on the self-healing performance of different mixes by conducting microstructure, mechanical properties, and durability experiments and also investigating self-healing ability under repeated flexural loads and sustained tensile loads. Two different mixes of UHPC incorporating varying ratios of SAP as well as a control mix without SAP were utilised for this study with three different curing regimes for each mix. The major findings from this study are as follows:

- Adding SAP to UHPC required additional water or superplasticiser to maintain the consistency of the mix where the required amount of water depended on the size and absorption capacity of SAP particles.

- UHPC mixed with SAP exhibited less compressive strength than the corresponding control mix without SAP, and the compressive strength exceeded above 120 MPa after 90 days for UHPC mixes with SAP. SAP leaves voids in the matrix after releasing the water, which could significantly impact the microstructure of the matrix. However, the release of the water later enhanced the hydration of the UHPC mix and led to the improvement in the strength.
- Adding SAP particles improved the modulus of elasticity by closing the microcracks, which led to the improvement in the stiffness.
- Regarding flexural and tensile strength results, S0.3 exhibited better results than the mix without SAP in water-cured specimens. There was a decrease in self-desiccation of the internal curing and a reduction in the occurrence of microcracks.
- The microstructure of the matrix of UHPC showed the formation of C-S-H gel around SAP voids. Hence, the formation of C-S-H should increase the strength.
- Notched specimens of UHPC mixed with SAP had an overall better performance in terms of load recovery and immediate closing of the cracks via the formation of calcite.
- Prisms under sustained tensile load for UHPC and S0.4 under wet and dry cycle conditions also confirmed the previous results of self-healing ability after adding SAP. The stress increased for S0.4 with time, indicating that the healing happened with constant displacement readings.
- UHPC had better compressive strength due to the dense microstructure in its early stages, and the addition of SAP reduced the compressive strength. However, the addition of SAP showed superior results in tensile and flexural strength tests and also the restoration of the stiffness of the healed concrete. Additionally, mixes with SAP had enhanced the healing process, which could be the cornerstone of more durable and sustainable concrete.

Finally, blending SAP into UHPC seems to have the potential of reduce the maintenance required, reduce the cost-related expenses, and increase the life-span of the buildings. However, Incorporating SAP into UHPC mixes investigation can be further investigated under an aggressive environment such as sulphate attacks. Moreover, the technique of testing the self-healing capability under sustained loadings can be expanded to extend the duration of the sustained loadings.

Author Contributions: Conceptualisation, M.A., M.M.A., M.E. and A.S.; Methodology, M.A., M.M.A., M.E. and R.F.; Software, M.A. and R.F.; Validation, M.A., M.M.A., M.E., A.S. and R.F.; Formal Analysis, M.A. and R.F.; Investigation, M.A., M.M.A. and R.F.; Resources, M.A., M.M.A., M.E., A.S. and R.F.; Data Curation, M.A., M.M.A. and R.F.; Writing—Original Draft Preparation, M.A., M.M.A., M.E., A.S. and R.F.; Writing—Review & Editing, M.A., M.M.A., M.E., A.S. and R.F.; Visualization, M.A. and R.F.; Supervision, M.M.A., M.E. and A.S.; Project Administration, M.A. and M.M.A.; Funding Acquisition, M.M.A. and M.E. All authors have read and agreed to the published version of the manuscript.

Funding: The research was partially funded by the Australian Research Council grant number [DP 21001425].

Data Availability Statement: Dataset available on request from the authors.

Acknowledgments: The authors would like to thank Phillip Visintin for using the test frame of sustained tensile loading experiment as well as Kevin Farries who designed the frame.

Conflicts of Interest: The authors declare no conflict of interest.

References

1. Graybeal, B.A.; Russel, H.G. *Ultra-High Performance Concrete: A State-of-the-Art Report for the Bridge Community*; United States. Federal Highway Administration. Office of Infrastructure Research and Development: McLean, VA, USA, 2013.
2. Xue, J.; Briseghella, B.; Huang, F.; Nuti, C.; Tabatabai, H.; Chen, B. Review of ultra-high performance concrete and its application in bridge engineering. *Constr. Build. Mater.* **2020**, *260*, 119844. [[CrossRef](#)]
3. Schmitz, G.M. Design and Experimental Validation of 328 ft (100 m) Tall Wind Turbine Towers Utilizing High Strength and Ultra-High Performance Concrete. Ph.D. Thesis, Iowa State University, Ames, IA, USA, 2013; p. 210.

4. Hajar, Z.; Resplendino, J.; Lecointre, D.; Petitjean, J.; Simon, A. Ultra-high-performance concretes: First recommendations and examples of application. In Proceedings of the Fib Symposium 2004—Concrete Structures: The Challenge of Creativity, Avignon, France, 26–28 May 2004; pp. 242–243.
5. Bonneau, O.; Vernet, C.; Moranville, M.; Aïtcin, P.C. Characterization of the granular packing and percolation threshold of reactive powder concrete. *Cem. Concr. Res.* **2000**, *30*, 1861–1867. [[CrossRef](#)]
6. Ji, T.; Chen, C.Y.; Zhuang, Y.Z. Evaluation method for cracking resistant behavior of reactive powder concrete. *Constr. Build. Mater.* **2012**, *28*, 45–49. [[CrossRef](#)]
7. Wang, K.; Jansen, D.C.; Shah, S.P.; Karr, A.F. Permeability study of cracked concrete. *Cem. Concr. Res.* **1997**, *27*, 381–393. [[CrossRef](#)]
8. American Concrete Institute. Control of Cracking in Concrete Structures. In *Concrete International*; American Concrete Institute: Farmington Hills, MI, USA, 1980; pp. 35–76. [[CrossRef](#)]
9. Raza, A.; El Ouni, M.H.; Azab, M.; Khan, D.; Elhadi, K.M.; Alashker, Y. Sustainability assessment, structural performance and challenges of self-healing bio-mineralized concrete: A systematic review for built environment applications. *J. Build. Eng.* **2023**, *66*, 105839. [[CrossRef](#)]
10. Van Tittelboom, K.; De Belie, N. Self-Healing in Cementitious Materials—A Review. *Materials* **2013**, *6*, 2182–2217. [[CrossRef](#)]
11. Guo, X.; Liu, X.; Yuan, S. Effects of initial damage on self-healing of fly ash-based engineered geopolymer composites (FA-EGC). *J. Build. Eng.* **2023**, *74*, 106901. [[CrossRef](#)]
12. Wang, R.; Ding, Z.; Zhang, Y.; Xu, Y. Self-healing of high-performance engineered cementitious materials with crystalline admixture in the seawater environment. *J. Build. Eng.* **2023**, *63*, 105472. [[CrossRef](#)]
13. Ma, X.; Liu, J.; Shi, C. A review on the use of LWA as an internal curing agent of high performance cement-based materials. *Constr. Build. Mater.* **2019**, *218*, 385–393. [[CrossRef](#)]
14. Zhang, Y.; Sun, X. Influence of multi-walled carbon nanotubes on the multi-scale performance of internally cured concrete containing pre-wetted lightweight aggregate. *J. Build. Eng.* **2022**, *58*, 104986. [[CrossRef](#)]
15. Liu, J.; Farzadnia, N.; Khayat, K.; Shi, C. Effects of SAP characteristics on internal curing of UHPC matrix. *Constr. Build. Mater.* **2021**, *280*, 122530. [[CrossRef](#)]
16. Wang, F.; Zhou, Y.; Peng, B.; Liu, Z.; Hu, S. Autogenous Shrinkage of Concrete with Super-Absorbent Polymer. *ACI Mater. J.* **2009**, *106*, 123. [[CrossRef](#)]
17. Liu, K.; Long, Y.; Chen, L.; Ling, X.; Yu, R.; Shui, Z.; Fei, S.; Yu, W.; Li, C.; Ge, K. Mechanisms of autogenous shrinkage for Ultra-High Performance Concrete (UHPC) prepared with pre-wet porous fine aggregate (PFA). *J. Build. Eng.* **2022**, *54*, 104622. [[CrossRef](#)]
18. Lee, H.X.D.; Wong, H.S.; Buenfeld, N.R. Self-sealing of cracks in concrete using superabsorbent polymers. *Cem. Concr. Res.* **2016**, *79*, 194–208. [[CrossRef](#)]
19. Craeye, B.; Geirnaert, M.; De Schutter, G. Super absorbing polymers as an internal curing agent for mitigation of early-age cracking of high-performance concrete bridge decks. *Constr. Build. Mater.* **2011**, *25*, 1–13. [[CrossRef](#)]
20. Mignon, A.; Vagenende, M.; Martins, J.; Dubruel, P.; Van Vlierberghe, S.; De Belie, N. Development of amine-based pH-responsive superabsorbent polymers for mortar applications. *Constr. Build. Mater.* **2017**, *132*, 556–564. [[CrossRef](#)]
21. Olawuyi, B.J. The Mechanical Behaviour of High-Performance Concrete with Superabsorbent Polymers (SAP). 2016. Available online: <http://hdl.handle.net/10019.1/98352> (accessed on 15 April 2023).
22. Pourjavadi, A.; Fakoorpoor, S.M.; Khaloo, A.; Hosseini, P. Improving the performance of cement-based composites containing superabsorbent polymers by utilization of nano-SiO₂ particles. *Mater. Des.* **2012**, *42*, 94–101. [[CrossRef](#)]
23. Savva, P.; Petrou, M.F. Highly absorptive normal weight aggregates for internal curing of concrete. *Constr. Build. Mater.* **2018**, *179*, 80–88. [[CrossRef](#)]
24. Kang, S.-H.; Hong, S.-G.; Moon, J. Shrinkage characteristics of heat-treated ultra-high performance concrete and its mitigation using superabsorbent polymer based internal curing method. *Cem. Concr. Compos.* **2018**, *89*, 130–138. [[CrossRef](#)]
25. Yang, Z.; Miao, C.; Deng, W.; Liu, D.; Zhang, J.; Gu, J. Multi-scale characterization of SAP impact on self-healing behavior in UHPC under varied crack widths and environments. *Constr. Build. Mater.* **2024**, *421*, 135649. [[CrossRef](#)]
26. Ma, X.; Yuan, Q.; Liu, J.; Shi, C. Effect of water absorption of SAP on the rheological properties of cement-based materials with ultra-low w/b ratio. *Constr. Build. Mater.* **2019**, *195*, 66–74. [[CrossRef](#)]
27. Samaha, H.R.; Hover, K.C. Influence of microcracking on the mass transport properties of concrete. *ACI Mater. J.* **1992**, *89*, 416–424. [[CrossRef](#)]
28. Hearn, N. Effect of Shrinkage and Load-Induced Cracking on Water Permeability of Concrete. *ACI Mater. J.* **1999**, *96*, 234–241. [[CrossRef](#)]
29. Grzybowski, M.; Shah, S.P. Shrinkage Cracking of Fiber Reinforced Concrete. *ACI Mater. J.* **1990**, *87*, 138–148. [[CrossRef](#)]
30. Liu, S.; Bundur, Z.B.; Zhu, J.; Ferron, R.D. Evaluation of self-healing of internal cracks in biomimetic mortar using coda wave interferometry. *Cem. Concr. Res.* **2016**, *83*, 70–78. [[CrossRef](#)]
31. Kan, L.L.; Shi, H.S.; Sakulich, A.R.; Li, V.C. Self-Healing Characterization of Engineered Cementitious Composite Materials. *ACI Mater. J.* **2010**, *107*, 619–626. [[CrossRef](#)]
32. Zhang, Z.; Qian, S.; Ma, H. Investigating mechanical properties and self-healing behavior of micro-cracked ECC with different volume of fly ash. *Constr. Build. Mater.* **2014**, *52*, 17–23. [[CrossRef](#)]

33. Kanellopoulos, A.; Giannaros, P.; Al-Tabbaa, A. The effect of varying volume fraction of microcapsules on fresh, mechanical and self-healing properties of mortars. *Constr. Build. Mater.* **2016**, *122*, 577–593. [[CrossRef](#)]
34. Ma, W.; Xu, Z.; Qin, Y.; Cao, C.; Wang, Y.; Zhou, H. Experimental investigation of nonlinear flow characteristics in cracked polypropylene fibre-reinforced concrete. *Mater. Struct.* **2021**, *54*, 215. [[CrossRef](#)]
35. Nishiwaki, T.; Koda, M.; Yamada, M.; Mihashi, H.; Kikuta, T. Experimental study on self-healing capability of FRCC using different types of synthetic fibers. *J. Adv. Concr. Technol.* **2012**, *10*, 195–206. [[CrossRef](#)]
36. Monte, F.L.; Ferrara, L. Tensile behaviour identification in Ultra-High Performance Fibre Reinforced Cementitious Composites: Indirect tension tests and back analysis of flexural test results. *Mater. Struct.* **2020**, *53*, 145. [[CrossRef](#)]
37. Ma, H.; Qian, S.; Zhang, Z. Effect of self-healing on water permeability and mechanical property of Medium-Early-Strength Engineered Cementitious Composites. *Constr. Build. Mater.* **2014**, *68*, 92–101. [[CrossRef](#)]
38. Roig-Flores, M.; Pirritano, F.; Serna, P.; Ferrara, L. Effect of crystalline admixtures on the self-healing capability of early-age concrete studied by means of permeability and crack closing tests. *Constr. Build. Mater.* **2016**, *114*, 447–457. [[CrossRef](#)]
39. Cuenca, E.; Tejedor, A.; Ferrara, L. A methodology to assess crack-sealing effectiveness of crystalline admixtures under repeated cracking-healing cycles. *Constr. Build. Mater.* **2018**, *179*, 619–632. [[CrossRef](#)]
40. Sahmaran, M.; Yildirim, G.; Noori, R.; ÖZBAY, E.; Lachemi, M. Repeatability and pervasiveness of self-healing in engineered cementitious composites. *ACI Mater. J.* **2015**, *112*, 513–522. [[CrossRef](#)]
41. Snoeck, D.; De Belie, N. Repeated Autogenous Healing in Strain-Hardening Cementitious Composites by Using Superabsorbent Polymers. *J. Mater. Civil. Eng.* **2016**, *28*, 4015086. [[CrossRef](#)]
42. ASTM C1437-20; Standard Test Method for Flow of Hydraulic Cement Mortar. ASTM International: West Conshohocken, PA, USA, 2020. [[CrossRef](#)]
43. Singh, M.; Sheikh, A.H.; Ali, M.S.M.; Visintin, P.; Griffith, M.C. Experimental and numerical study of the flexural behaviour of ultra-high performance fibre reinforced concrete beams. *Constr. Build. Mater.* **2017**, *138*, 12–25. [[CrossRef](#)]
44. ASTM C39/C39M-20; Standard Test Method for Compressive Strength of Cylindrical Concrete Specimens. ASTM International: West Conshohocken, PA, USA, 2020. [[CrossRef](#)]
45. ASTM C642-21; Standard Test Method for Density, Absorption, and Voids in Hardened Concrete. ASTM International: West Conshohocken, PA, USA, 2021. [[CrossRef](#)]
46. ASTM C1585-20; Standard Test Method for Measurement of Rate of Absorption of Water by Hydraulic-Cement Concretes. ASTM International: West Conshohocken, PA, USA, 2020. [[CrossRef](#)]
47. Feng, Z.; Li, C.; Yoo, D.-Y.; Pan, R.; He, J.; Ke, L. Flexural and cracking behaviors of reinforced UHPC beams with various reinforcement ratios and fiber contents. *Eng. Struct.* **2021**, *248*, 113266. [[CrossRef](#)]
48. Mechtcherine, V.; Secieru, E.; Schröfl, C. Effect of superabsorbent polymers (SAPs) on rheological properties of fresh cement-based mortars—Development of yield stress and plastic viscosity over time. *Cem. Concr. Res.* **2015**, *67*, 52–65. [[CrossRef](#)]
49. Liu, J.; Farzadnia, N.; Shi, C.; Ma, X. Shrinkage and strength development of UHSC incorporating a hybrid system of SAP and SRA. *Cem. Concr. Compos.* **2019**, *97*, 175–189. [[CrossRef](#)]
50. Snoeck, D.; Schaubroeck, D.; Dubruel, P.; De Belie, N. Effect of high amounts of superabsorbent polymers and additional water on the workability, microstructure and strength of mortars with a water-to-cement ratio of 0.50. *Constr. Build. Mater.* **2014**, *72*, 148–157. [[CrossRef](#)]
51. Snoeck, D.; Van Tittelboom, K.; Steuperaert, S.; Dubruel, P.; De Belie, N. Self-healing cementitious materials by the combination of microfibrils and superabsorbent polymers. *J. Intell. Mater. Syst. Struct.* **2014**, *25*, 13–24. [[CrossRef](#)]
52. Kovler, K. Effect of superabsorbent polymers on the mechanical properties of concrete. In *Application of Super Absorbent Polymers (SAP) in Concrete Construction: State-of-the-Art Report Prepared by Technical Committee 225-SAP*; Springer: Dordrecht, The Netherlands, 2012; pp. 99–114. [[CrossRef](#)]
53. Assmann, A.; Reinhardt, H.W. Tensile creep and shrinkage of SAP modified concrete. *Cem. Concr. Res.* **2014**, *58*, 179–185. [[CrossRef](#)]
54. Qian, S.Z.; Zhou, J.; Schlangen, E. Influence of curing condition and precracking time on the self-healing behavior of Engineered Cementitious Composites. *Cem. Concr. Compos.* **2010**, *32*, 686–693. [[CrossRef](#)]
55. Darquennes, A.; Olivier, K.; Benboudjema, F.; Gagné, R. Self-healing at early-age, a way to improve the chloride resistance of blast-furnace slag cementitious materials. *Constr. Build. Mater.* **2016**, *113*, 1017–1028. [[CrossRef](#)]
56. Jensen, O.M.; Hansen, P.F. Water-entrained cement-based materials—I. Principles and theoretical background. *Cem. Concr. Res.* **2001**, *31*, 647–654. [[CrossRef](#)]
57. Zhutovsky, S.; Kovler, K. Durability aspects of internally cured high performance concrete. In Proceedings of the International RILEM Conference on Use of Superabsorbent Polymers and Other New Additives in Concrete, Lyngby, Denmark, 15–18 August 2010; pp. 15–18.
58. Sun, B.; Wu, H.; Song, W.; Li, Z.; Yu, J. Hydration, microstructure and autogenous shrinkage behaviors of cement mortars by addition of superabsorbent polymers. *Front. Struct. Civ. Eng.* **2020**, *14*, 1274–1284. [[CrossRef](#)]
59. Snoeck, D.; Dewanckele, J.; Cnudde, V.; De Belie, N. X-ray computed microtomography to study autogenous healing of cementitious materials promoted by superabsorbent polymers. *Cem. Concr. Compos.* **2016**, *65*, 83–93. [[CrossRef](#)]

-
60. Sun, J.; Shi, H.; Qian, B.; Xu, Z.; Li, W.; Shen, X. Effects of synthetic C-S-H/PCE nanocomposites on early cement hydration. *Constr. Build. Mater.* **2017**, *140*, 282–292. [[CrossRef](#)]
 61. Bentz, D.P.; Jensen, O.M. Mitigation strategies for autogenous shrinkage cracking. *Cem. Concr. Compos.* **2004**, *26*, 677–685. [[CrossRef](#)]

Disclaimer/Publisher’s Note: The statements, opinions and data contained in all publications are solely those of the individual author(s) and contributor(s) and not of MDPI and/or the editor(s). MDPI and/or the editor(s) disclaim responsibility for any injury to people or property resulting from any ideas, methods, instructions or products referred to in the content.